X-Rays

William Bidle and Beatrice Liang-Gilman
Department of Physics and Astronomy, Rutgers University
(Dated: 9 November 2020)

Abstract We study the phenomena of x-ray powder-pattern diffraction in different alloys to verify Vegard's Law for copper-nickel alloys and use these findings to determine the nickel content of some American and Canadian nickel coins. We find that American nickels contain (25.95 $\pm$ 4.43)% nickel, 1979 Canadian nickels contain (101.05 $\pm$ 4.11)% nickel, and 1984 Canadian nickels contain (30.53 $\pm$ 4.42)% nickel. The same techniques are also used to identify an unknown sample, and by comparing our measurements against the theoretical expectations of various metals with similar properties, we determine our unknown sample to be Molybdenum.

I. INTRODUCTION AND THEORY

When a collimated beam of x-rays strike pairs of parallel lattice planes in a crystal, each atom acts as a scattering center and emits a secondary wave (see Figure 1). Under specific conditions, the reflected radiation off of these peaks will constructively interfere with one another, and the phenomena is described by Bragg's Law:

$$n\lambda = 2d_{hkl}\sin(\theta)$$

Here, λ is the wavelength of the x-ray beam, θ is the angle of incidence with respect to the Bragg plane, n is an integer representing the diffraction order, and d_{hkl} represents the distance between adjacent Bragg planes. Bragg planes are the set of equidistant parallel planes that pass through all the atoms in the crystal, and are represented by the Miller indices h, k, and l. The h, k, and l Miller indices correspond respectively to the x, y, and z components of a vector perpendicular to the plane. Figure 2 shows different sets of Bragg planes and their corresponding Miller indices.

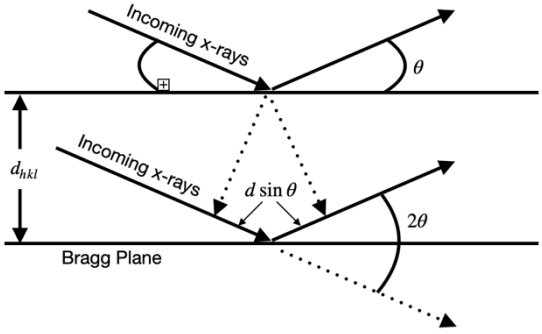

Figure 1: Visual representation of x-ray diffraction and Bragg's Law. The x-ray beam is incident on parallel Bragg planes and results in a diffraction pattern under certain conditions.

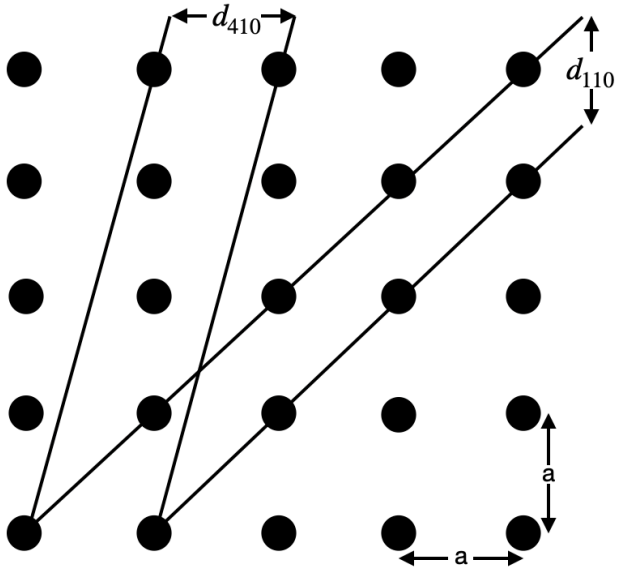

Figure 2: Bragg planes in a cubic solid

For cubic crystals, the distance between adjacent Bragg planes is:

$$d_{hkl} = \frac{a}{\sqrt{h^2 + k^2 + l^2}}$$

The lattice constant *a* represents the distance between ions at the corners of the cube. Each cubic crystal has multiple sets of Bragg planes (coming from different allowed combinations of Miller indices), which account for the multiple peaks that are seen when the x-ray beams hits the crystal at different angles.

The ions in crystalline materials take up specific positions in a lattice formation. Crystalline structures come in several forms, such as the simplest cubic structure, the body-centered cubic (BCC) structure, the face-centered cubic (FCC) structure, and the FCC diamond structure.

In this experiment, we test how the lattice constant varies for different alloys of copper in nickel. Since copper is totally soluble in nickel, copper-nickel alloys can be formed with any ratio. Given that we know the lattice constants of copper and nickel, and x is the number fraction of copper ions between 0 and 1, Vegard's Law gives us the lattice constant of the copper-nickel alloy:

$$a_{alloy} = xa_{Cu} + (1 - x)a_{Ni}$$

The magnetism of the copper-nickel alloy can also be predicted, as copper by itself is nonmagnetic, and nickel is a magnetic element with a Curie point of $T_C = 368°$. The Curie point of Cu_xN_{1-x} alloys is:

$$T_C = 368 - 1170x\ (°C)$$

Implying that samples with more than 30% copper are not magnetic at room temperature.

To study x-ray diffraction in crystals, both the Laue method and the power method can be used. For the Laue method, an x-ray beam with a continuous distribution of x-ray wavelengths is used with a single crystal sample. The incident beam then makes the same angle with all parts of the sample and the angle of incidence is fixed. The Laue method is useful in studying crystals but can be hard to interpret. In contrast, the powder method uses monochromatic x-rays on a finely powdered sample. Even though this forces the wavelength to be fixed, it is still able to produce the diffraction pattern since the many small crystallites are randomly oriented. A detector is rotated from 0° to 180° around the sample, while the sample itself rotates from 0° to 90° to measure all angles. The benefit of using the powder method is it is easier to interpret and produces a more accurate spectrum. For this experiment, we use the powder method to study x-ray diffraction spectrums and analyze the composition of different alloys.

This experiment uses characteristic x-rays as opposed to bremsstrahlung. To produce the x-rays in this experiment, a beam of electrons is accelerated across a large potential difference into a water-cooled copper target. If the electrons pass close enough to the nuclei in the target, they are deflected and slowed down by the attractive force of the nucleus in a process called bremsstrahlung. The lost kinetic energy appears as an x-ray photon, where each photon can have a different amount of energy, leading to a continuous distribution of bremsstrahlung wavelengths. In comparison, characteristic x-rays are formed when the high-speed electrons collide with orbital electrons in the target, knocking the orbital electrons out. A higher energy level electron then takes its place and emits the extra energy as an x-ray photon. Consequently, characteristic x-rays provide narrower lines that are more useful for the powder method.

Finally, as crystal structure becomes increasingly symmetric, x-rays diffracted from some planes experience total destructive interference. This is why for BCC and FCC structure, which are more complex cubic structures, not all peaks will show up that would appear for a solid with a simple cubic structure. The indices where total destructive interference occurs are called "missing lines/peaks". Diamond structures have even more missing lines than FCC structures, since their structures look like two interlapping FCC structures.

II. APPARATUS AND PROCEDURE

The experimental apparatus can be seen in Figure 3 below. The device used to perform the experiment was a Rigaku 30 kV Miniflex powder pattern x-ray spectrometer. The sample to be studied is swept by the built-in goniometer through an angle θ with respect to the x-ray beam, while the detector is swept through an angle of 2θ[1].

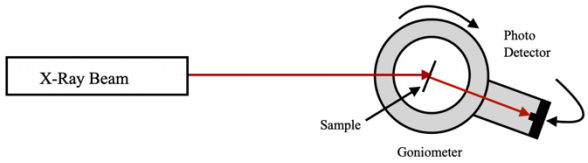

Figure 3: A schematic of the experimental setup viewed from above

In order to accurately determine the 2θ angle at which there was a detected index line (a peak), we decided to use a gaussian fit to each individual peak. The overall shape and behavior of these peaks closely resembled gaussian behavior, and since gaussian functions are symmetric, we could simply use the maximum value of the fit to determine the 2θ angle. This method turned out to be very accurate since the number of data points used in the fit was large (~30000).

The first thing to do for the experiment was to find the x-ray spectrum for a silicon sample from 20° to 80° at 2° per minute. Given that silicon has a diamond structure with a lattice constant of 5.4309 Å, the theoretical values for where the peaks should appear can be calculated with Bragg's Law. The comparison between theoretical and experimental values serve as a reference for the remainder of the experiment to help determine errors in the system and setup.

Once the silicon x-ray spectrum was recorded, a full sweep (from 0° to 160° at 2°/min) of a Cu-Si sample was taken to

[1] The goniometer sweeps in the direction of decreasing 2θ.

establish the full spectrum of copper. Due to the difference in reaction time between starting the data collection and starting the goniometer, the presence of the silicon peaks was used to shift the whole measured spectrum comparing to their theoretical values. After the shift, the copper peaks were then compared to their theoretical values, which were calculated using the known lattice constant of 3.6153 Å (see [1]). The predicted values of 2θ can be seen in Table 1.

Copper ($a = 3.6153$ Å, $\lambda = 1.5418$ Å)		
Index	$\frac{\lambda\sqrt{h^2+k^2+l^2}}{2a}$	2θ (degrees)
111	0.369	43.349
200	0.426	50.487
220	0.603	74.186
311	0.707	90.017
222	0.739	95.235
400	0.853	117.064
331	0.929	136.701
420	0.954	144.958

Table 1: Calculated expectations of 2θ for copper.

A similar process was then performed for a Ni-Si sample to establish the full spectrum of nickel. In order to make the process more efficient, the theoretical values for the nickel peaks were calculated prior to taking data, and data was only taken in the ranges where peaks were expected to be seen. The nickel peak values were then compared to their theoretical counterparts using a lattice constant of 3.5238 Å (see [1]). The predicted values of 2θ can be seen in Table 2.

Nickel ($a = 3.5238$ Å, $\lambda = 1.5418$ Å)		
Index	$\frac{\lambda\sqrt{h^2+k^2+l^2}}{2a}$	2θ (degrees)
111	0.379	44.534
200	0.438	51.894
220	0.619	76.453
311	0.726	93.034
222	0.758	98.548
400	0.875	122.108
331	0.954	144.953
420	0.978	156.121

Table 2: Calculated expectations of 2θ for nickel.

Once the full x-ray spectrums for both copper and nickel were recorded, the lowest two index lines, (111) and (200), of each were then closely compared. Given that both elements have an FCC structure and similar lattice constant value, they should have similar peak values (within 1.5% of each other as seen above). A sweep from 40° to 55° at 0.5°/min was performed to capture both peaks for each sample, as well as the silicon (220) peak to be used as a reference. The slower sweep was used to provide a more accurate measurement of the peak 2θ values. From these measurements, the lattice constant can then be calculated using each peak value and Bragg's Law. The values were then averaged and compared to the accepted values from [1].

Following this, we moved on to look at Cu-Ni alloys. We used three different alloy samples, each with a different concentration of copper and nickel[2], each with a small portion of silicon on them for reference. Sweeping from 43° to 48° at 0.5°/min, data was recorded for the alloy (111) line and silicon (220) line for each sample. Using the silicon line to shift the spectrum accordingly, the lattice constant of the alloy can then be calculated using Vegard's Law and the provided concentrations of copper and nickel. These lattice constants were then plotted as a function of copper concentration, fitted with a least square fit, and compared to the theoretical equation. Each sample was also held up to a horseshoe magnet to determine which of the alloys were magnetic, comparing with the expectations derived from the Cu-Ni Curie point.

To expand on the examination of alloys, three different nickels were studied: a U.S. nickel, a 1979 Canadian nickel, and a 1984 Canadian nickel. This time, the copper and nickel concentrations were not known ahead of time and were to be determined. Each nickel sample had some silicon on it to use as a reference point. We used the same sweep on the nickels as in the previous step, from 43° to 48° at 0.5°/min to use the Cu-Ni alloy (111) peak in our analysis. After shifting the spectrum according to the location of the measured silicon (220) peak, the location of the alloy peak could be used in Bragg's Law to find the lattice constant of the alloy. Then, Vegard's Law was used to find the corresponding copper and nickel concentrations for each nickel. In addition, each nickel was tested for magnetism, and compared to theoretical predictions.

Finally, we recorded the x-ray spectrum of an unknown element to try to uncover what the element was. The mass and volume were first measured in order to calculate its density to narrow down the list of possible elements. The unknown sample was then swept from 35° to 105° at 2°/min to find the 2θ values of each peak. With no silicon component to create reference peaks from, the error from the original silicon measurements was incorporated to account for errors in the goniometer and reaction time. After finding the values of each peak, the peak theta values were plotted as a function of peak number. These were then compared to

[2] The Cu:Ni ratio for the alloys used were 0.82:0.18, 0.53:0.47, and 0.26:0.74. The error in these given concentrations is assumed to be 2%.

theoretical plots of various elements that had density values close to what was measured for this unknown sample. By comparing the observed peak theta values with the theoretical ones, we were able to narrow down what the unknown element was with high confidence.

III. DATA ANALYSIS

Part 2: Si Spectrum

The x-ray spectrum for silicon, sweeping 2θ at 2° per minute from 20° to 80° can be seen in Figure 4 below. A zoom in on each of the peaks, as well as a gaussian fit to each peak is also included and can be seen in Figure 5.

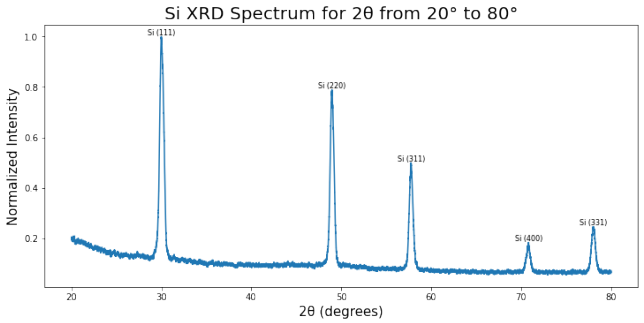

Figure 4: XRD spectrum for Silicon sweeping 2θ from 20° to 80°

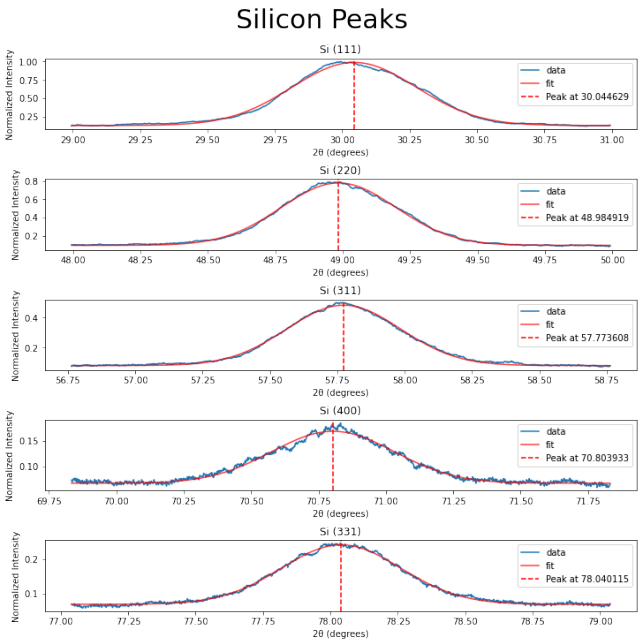

Figure 5: Zoom in of the Silicon XRD Peaks and their 2θ values

It can be seen in Figure 3 that five strong and sharp intensity peaks appear in the range 20° to 80°. Each of these peaks correspond to different index lines, and the exact measurements can be seen in Figure 5 from the gaussian fit. A comparison between our experimental results and theoretical expectations can be seen in Table 3 below. Each of the measured peak values falls on average about 1.606° outside of the expected value for 2θ. Fortunately, this is common for all of the peaks, and must be a result of error coming from goniometer misalignment, angle at which the beam hits the detector, and reaction time. This average difference could then be used for later scans when no silicon peaks are present.

Silicon Spectrum Analysis					
Index	(111)	(220)	(311)	(400)	(331)
Normalized Intensity	1.000	0.787	0.500	0.184	0.246
	2θ (degrees)				
Experiment	30.045	48.985	57.774	70.804	78.040
Theory	28.465	47.342	56.171	69.192	76.447
Difference	1.580	1.643	1.603	1.612	1.593
Average Difference	1.606				
Std Dev	0.021				

Table 3: Comparison of experimental results and theoretical expectations for the XRD spectrum of silicon for 2θ at 2° per minute from 20° to 80° (angular measurements are in terms of 2θ)

Part 3: Cu and Ni Spectrums

The x-ray spectrum for a Cu-Si sample sweeping 2θ at 2° per minute from 20° to 160°, along with the labeled index lines, can be seen in Figure 6 below. The individual peaks are labeled with their corresponding Miller indices, and a gaussian fit was done to determine the values of 2θ as accurately as possible.

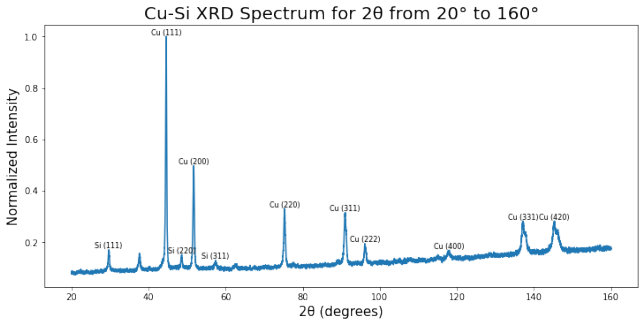

Figure 6: XRD spectrum for Ci-Si sample sweeping 2θ from 20° to 160°

In this case, since there were three noticeable silicon peaks present, we decided to use the average deviation of these peaks from their theoretical values to shift the copper 2θ values by 1.499° with an error of 0.393°. Note that this is relatively close to the average deviation calculated in part one with the 5 silicon peaks, however the values are different enough to see that each individual measurement results in a

different amount to be shifted by[3]. It can also be noted that there is an unlabeled peak around 40°, which is not in agreement with either the silicon or copper expectation values. We believe this extraneous peak could be due to the presence of oxidized copper, however it is unrelated to our study and does not impact the results. Table 4 shows the results of the 2θ copper peaks in relation to the theoretical expectations. The first three values fall within error (mentioned above) of expectation, however all of the following values do not. It can be seen that they deviate more from the expectation as 2θ get larger, potentially indicating a non-constant rotation speed of the goniometer, along with a splitting of the x-ray spectrum for the large values of 2θ. This splitting can actually be seen for the (420) and (331) lines in Figure 6.

Index	Theoretical 2θ (degrees)	Measured 2θ (degrees)	Difference (degrees)	Normalized Intensity
(111)	43.349	43.085	0.263	1.000
(200)	50.487	50.224	0.263	0.498
(220)	74.186	73.802	0.384	0.331
(311)	90.017	89.531	0.486	0.316
(222)	95.235	94.709	0.525	0.195
(400)	117.064	116.412	0.651	0.169
(331)	136.701	135.847	0.854	0.283
(420)	144.958	144.082	0.876	0.283

Table 4: Comparison of experimental results and theoretical expectations for the XRD spectrum of copper for 2θ at 2° per minute from 20° to 160° (angular measurements are in terms of 2θ)

The x-ray diffraction spectrum for the Ni-Si sample, along with the labeled index lines, can be seen in Figure 7 below. In this case, only ranges surrounding the expected theoretical peak values were swept at a speed of 2° per minute.

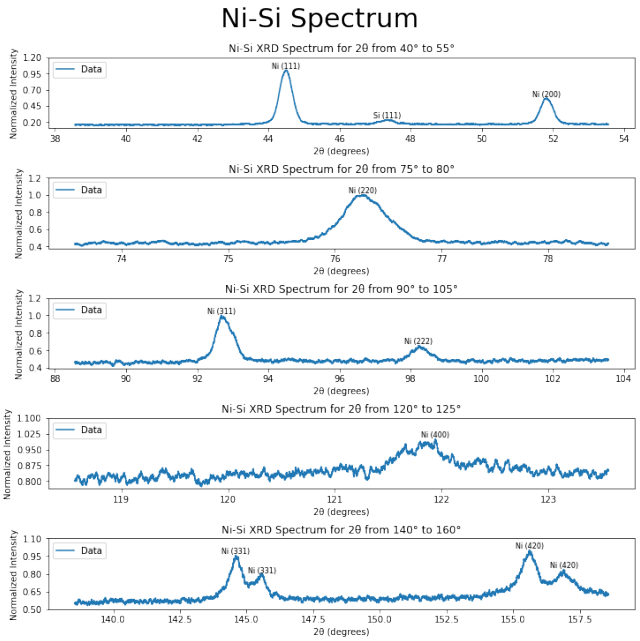

Figure 7: Ni-Si Spectrum for predetermined 2θ ranges at 2° per minute

To index the nickel spectrum, the difference of the theoretical peak and the silicon peak in the first spectrum range was used (1.437° with an error of 0.021°). The error was taken from the average of the shifted silicon peaks from the first part, as the systematic error. We can assume each nickel peak is shifted by about the same amount because each range of data was taken in the same manner in the same period of time. As can be seen in the spectrums above, there are eight nickel peaks and one silicon peak located in between the first two nickel lines. A comparison of these peaks with their theoretical values is done in Table 5 below. All of the theoretical theta values fall within error or very close to the error of the measured values. Notice that the Ni (331) line looks like two lines due to the two source lines from the x-ray. Usually, the difference in wavelength of the emitted x-rays (0.15406 nm and 0.15444 nm) is small enough to ignore, though at large values of 2θ, we can see a splitting of the x-ray spectrum, such as what occurs at the Ni (331) line. This can also be seen in the Ni (420) line. To confirm that this was in fact the case, a comparison of each peak's theta value and the theoretical values with the adjusted wavelengths was done and shown in the Appendix. However, for the purposes of the following table, the average theta value of the split peaks was used to compare against the theoretical values using the averaged wavelength.

[3] The discrepancy arises because the difference accounts for reaction time and alignment errors.

Index	Theoretical 2θ (degrees)	Measured 2θ (degrees)	Difference (degrees)	Normalized Intensity
(111)	44.534	44.496	0.037	1.000
(200)	51.894	51.831	0.063	0.568
(220)	76.453	76.273	0.180	0.394
(311)	93.034	92.770	0.264	0.400
(222)	98.5483	98.277	0.271	0.261
(400)	122.108	121.825	0.283	0.484
(331)	144.953	145.008	0.054	0.285
(420)	156.121	156.234	0.113	0.407

Table 5: Comparison of experimental results and theoretical expectations for the XRD spectrum of nickel for 2θ at 2° per minute (angular measurements are in terms of 2θ)

Part 4: Lowest Index Lines of Cu and Ni

The x-ray diffraction spectrum for the lowest two copper and nickel index lines can be seen in Figure 8 and Figure 9 respectively. For this scan we used a Cu-Si sample and a Ni-Si sample and scanned 2θ at 0.5° per minute from 40° to 55°. This range allowed us to capture the two lowest index lines for the materials of interest as well as the (220) index line for silicon to use as a reference point.

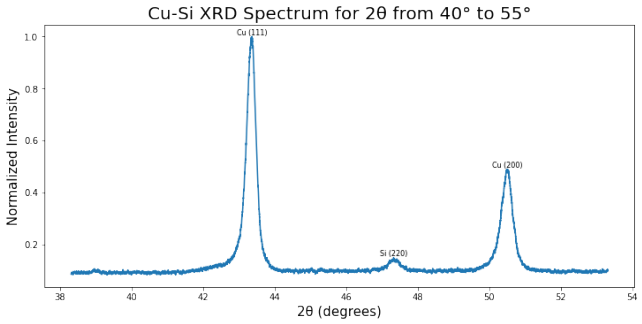

Figure 8: XRD spectrum for Ci-Si sample sweeping 2θ at 0.5° per minute from 40° to 55°. Note that the spectrum has been shifted slightly to the left due to the silicon peak correction.

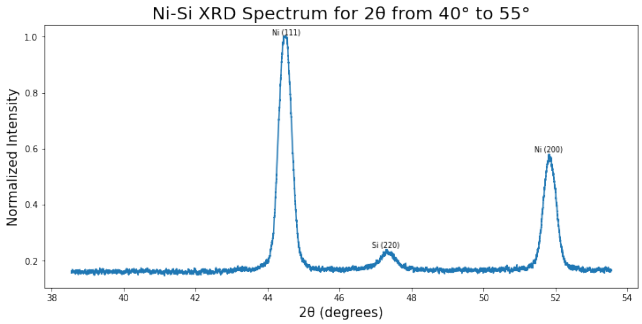

Figure 9: XRD spectrum for Ni-Si sample sweeping 2θ at 0.5° per minute from 40° to 55°. Note that the spectrum has been shifted slightly to the left due to the silicon peak correction.

Table 6 below shows the numerical results for each of the lowest index lines for both copper and nickel. The results have been adjusted based off of the deviation of the measured silicon (220) peak to the theoretical expectations.

Copper and Nickel (111) and (200) Analysis		
Index	(111)	(200)
Cu Measured	43.345°	50.494°
Cu Theory	43.349°	50.487°
a_{Cu}	(3.6156 ± .0040) Å	(3.6150 ± .0033) Å
a_{Cu} **Cullity**	3.6153 Å	
Ni Measured	44.490°	51.848°
Ni Theory	44.533°	51.894°
a_{Ni}	(3.5271 ± .0038) Å	(3.5267 ± .0032) Å
a_{Ni} **Cullity**	3.5238 Å	

Table 6: Comparison of experimental results and theoretical expectations for the XRD spectrum of Cu-Si and Ni-Si for 2θ at 0.5° per minute from 40° to 55° (angular measurements are in terms of 2θ)

The error reported above was determined by doing error propagation[4] of the uncertainty in 2θ to get an uncertainty in the lattice constant:

$$\sigma_a = a * \cot(\theta) * \sigma_\theta$$

Where θ and σ_θ are the measured angle and inherent error in the goniometer respectively. Note that θ is half of 2θ, which is what is measured in the experiment. Since the smallest increment on the goniometer is 0.1° (for 2θ), then the error in 2θ from alignment would be 0.05°, adopting the standard practice. Therefore, we define σ_θ to be 0.025°, resulting in the errors determined above. As seen in Table 6, each of the calculated values falls within the expected lattice constants listed in [1].

Part 5: Verification of Vegard's Law

Figure 10 below shows the experimental validation of Vegard's Law, based off of 5 different Cu:Ni concentrations. Two of the samples were based off of the (111) results in Part 4, using both a pure copper and pure nickel sample to better fit the data. For each of the three alloys, we scanned 2θ at 0.5° per minute from 48° to 43° to capture the (111) alloy peak, as well as the (220) silicon peak, the latter of which was used to shift the alloy peak.

[4] $\sigma_a = \frac{\partial a}{\partial \theta}\sigma_\theta$ since θ is the only dependent variable

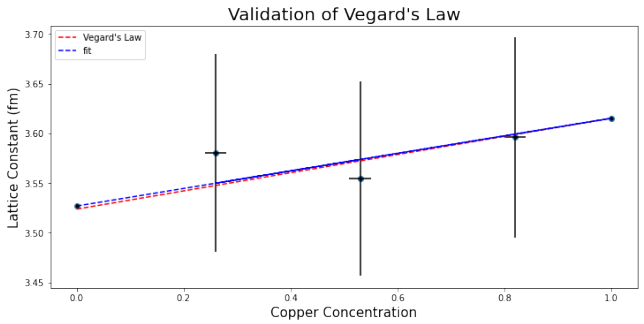

Figure 10: Plot of calculated lattice constants for the different alloys in relation to Vegard's Law.

The error in the lattice constant of each sample was determined by using σ_a defined in Part 4, again taking σ_θ to be 0.025°. The concentrations of each alloy were also taken to be within 2% of the given value, hence the error for only three of the data points. It can be seen that each of the calculated lattice constants for each alloy as well as the fit of the data fall well within the expectation of Vegard's Law. Each of the samples were also tested to see if any were magnetic by placing them in the center of a horseshoe magnet.

Ni Concentration	Cu Concentration	Magnetic?	Predicted to be magnetic?
$0.18 \pm .02$	$0.82 \pm .02$	no	no
$0.47 \pm .02$	$0.53 \pm .02$	yes	no
$0.74 \pm .02$	$0.26 \pm .02$	yes	yes

Table 7: Results for whether copper-nickel alloys are magnetic along with predictions.

As predicted, the alloy with less than 30% copper concentration was magnetic. In addition, the alloy with 82% copper was nonmagnetic as predicted. However, the alloy with 53% copper was magnetic where it was predicted to be nonmagnetic. A possible reason for this could be due to the sample being mislabeled with the incorrect concentration, having less copper than reported.

Part 6: Determination of Coin Concentrations

To examine different nickel coins, a sweep of a U.S. nickel, a 1979 Canadian nickel, and a 1984 Canadian nickel were taken at 0.5° per minute from 43° to 48°. Since the coins were formed with nickel-copper alloys, the (111) line was expected to show up in this range somewhere between the (111) lines for nickel and copper. In addition, the silicon on each coin produced a Si (220) line that was used as a reference for systematic errors.

Nickel Type	Lattice Constant (Å)	Ni Concentration (%)	Expected Ni Concentration
U.S.	$3.5923 \pm .0039$	25.95 ± 4.43	25%
1979 Canadian	$3.5228 \pm .0038$	101.05 ± 4.11	100%
1984 Canadian	$3.5882 \pm .0039$	30.53 ± 4.42	25%

Table 8: Comparison of the compositions of different nickel coins along with their expected values.

Once the spectrum was shifted according to the silicon peak, the angles at which the (111) line of the alloys were found. These values were then used in Bragg's Law to solve for the lattice constant a. Then, the measured lattice constant was used in Vegard's Law to find the copper and nickel concentrations of each coin. The US nickel has a nickel concentration of 25.95% that is consistent with expected results within given errors. The 1984 Canadian nickel's nickel concentration is also relatively close to the expected value at 30.53%. The fact that this value falls slightly outside of error bounds is most likely due to the nickel sample, which was not flush against the silicon coating. Upon closer inspection of the x-ray diffraction spectrum, which is shown in the Appendix, one can see the silicon line did not produce as smooth a curve to determine where the silicon peak lies.

The 1979 Canadian nickel produced a 101.05% nickel concentration, which is technically impossible. However, this impossible percentage arises from the alloy (111) line being located 0.013° to the right of the Ni (111) line, and therefore not between the Cu (111) and Ni (111) lines. This discrepancy could be credited to the loose nickel sample, where the silicon did not properly coat the nickel and the nickel could have shifted slightly while being rotated. Still, this 101.05% can reasonably be assumed to signify that the coin is completely composed of nickel, and is within error of the expected nickel concentration.

In addition, each nickel followed expected magnetism rules. The U.S. nickel and the 1984 Canadian nickel, which both have 75% copper, are not magnetic as predicted. On the other hand, the 1979 Canadian nickel is magnetic with 0% copper, as predicted since it has less than 30% copper.

Part 7: Unknown Sample

Finally, the x-ray diffraction spectrum of an unknown sample was taken using a sweep of 2° per minute from 35° to 105°, as seen below in Figure 11.

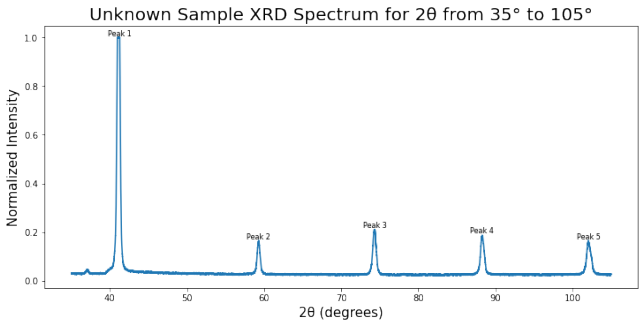

Figure 11: XRD spectrum for the unknown sample sweeping 2θ at 2° per minute from 35° to 135°.

To determine what element the unknown sample was, the mass and volume were first measured to find its density. The density was found to be $(10.32 \pm .02)\ \mathrm{g/cm^3}$, which was compared to known elemental density values found in [1], and found to be most similar to molybdenum and silver. The error in the density was calculated using error propagation:

$$\sigma_\rho = \rho\sqrt{(\frac{\sigma_M}{M})^2 + (\frac{\sigma_V}{V})^2}$$

$$\text{where } \sigma_V = V\sqrt{(\frac{\sigma_w}{w})^2 + (\frac{\sigma_l}{l})^2 + (\frac{\sigma_h}{h})^2}$$

Here, l, h, and w represent the dimensions of the sample that form the volume ($V = l * h * w$), M is the mass, and ρ is the density (along with their respective errors).

The theoretical lines for these two elements were then calculated (shown in the Appendix), given that molybdenum has a BCC structure and silver has an FCC structure. The different structures will have different missing lines, so corresponding peaks will not represent the same index lines in each spectrum. The peak theta values of the unknown element were then plotted against peak number alongside the theoretical values of molybdenum and silver, as shown in Figure 12.

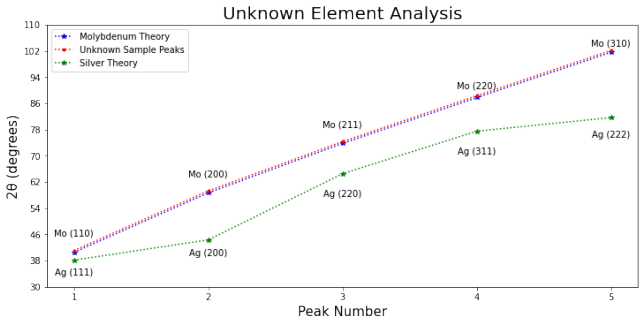

Figure 12: Analysis of the unknown sample peak locations vs peak number, comparing it to Molybdenum and Silver

From this plot, it can be easily seen that the unknown element is molybdenum, as the measured peak theta values correspond quite well to the theoretical values. In addition, each molybdenum theoretical value differs from the measured peak theta values by values between 0.55°-0.6°, so once the spectrum is shifted the peak values are within error bars calculated using the systematic error originally found in the silicon sample.

IV. CONCLUSION

From our experimental findings, we conclude that Bragg's Law accurately describes the phenomena of x-ray diffraction in the powder method. Our data agrees very well with theoretical predictions, and we were able to identify our unknown sample with confidence. A possible source of further error from the experiment could have come from misalignment of the detector with respect to the x-ray beam. We can do our best to line up the beam with the florescent paddle, however since some of the samples were not perfectly flat, it is hard to tell whether or not the reflected beam was well aligned.

This was most apparent in our data of the coins, where the Canadian coins were loose and the silicon coating did not overlap the coin. In order to further investigate this matter, a wider range of 2θ could be swept so more of the x-ray diffraction peaks appear. This would provide a more comprehensive analysis and give a more accurate error.

In addition, the error resulting from the difference in reaction time between starting data collection and starting the goniometer rotation could be lessened by the presence of two people. While circumstances made this impossible for our experiment, allowing two people to be present would not just lessen but also produce a consistent reaction time between the two actions.

V. REFERENECES

[1] B.D. Cullity: Elements of X-ray Diffraction, Addison-Wesley, Reading, Mass. 1978

VI. APPENDIX

Raw data gathered from our experiment can be found in the figures below, as well as the confirmation that the split peaks were caused by different wavelengths of emitted x-rays.

Split Peaks

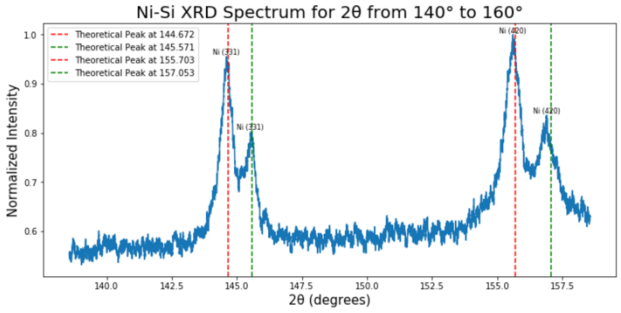

Figure 13: Shifted XRD spectrum of Ni-Si sample sweeping 2θ at 2° per minute from 140° to 160°. The red lines represent the theoretical 2θ values using a wavelength of 1.5406 Å, and the green lines represent the theoretical 2θ values using a wavelength of 1.5444 Å. Based on how close each theoretical value is to the split peaks, it can safely be assumed that these multiple peaks are due to the difference in emitted x-ray wavelengths.

Raw Coin Data

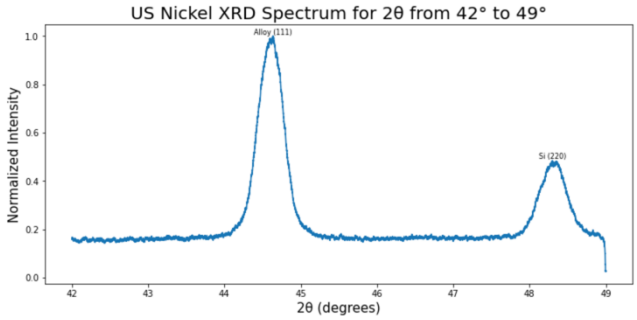

Figure 14: Raw data of XRD spectrum of US nickel coin sample sweeping 2θ at 0.5° per minute from 42° to 49°.

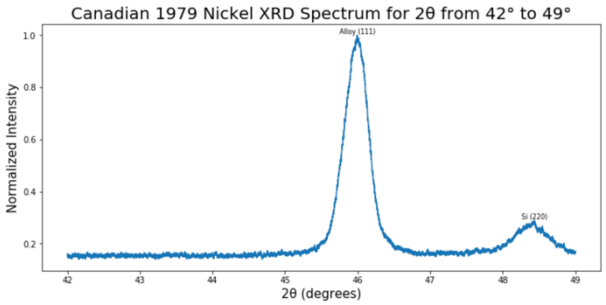

Figure 15: Raw data of XRD spectrum of Canadian 1979 nickel coin sample sweeping 2θ at 0.5° per minute from 42° to 49°.

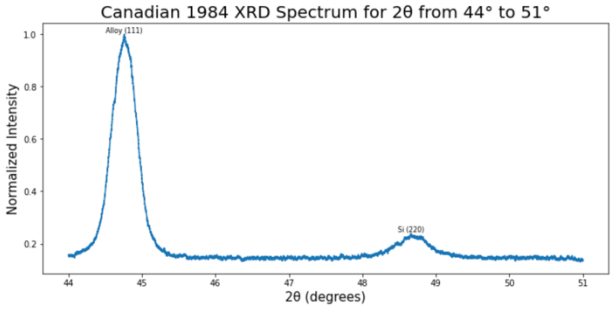

Figure 16: Raw data of XRD spectrum of Canadian 1984 nickel coin sample sweeping 2θ at 0.5° per minute from 44° to 51°.

Theoretical Peak Values

Molybdenum ($a = 3.1466$ Å, $\lambda = 1.5418$ Å)		
Index	$\frac{\lambda\sqrt{h^2+k^2+l^2}}{2a}$	2θ (degrees)
110	0.346	40.544
200	0.490	58.680
211	0.600	73.756
220	0.693	87.728
310	0.775	101.563
222	0.849	116.138

Table 9: Calculated expectations of 2θ for molybdenum with BCC structure.

Silver ($a = 4.086$ Å, $\lambda = 1.5418$ Å)		
Index	$\frac{\lambda\sqrt{h^2+k^2+l^2}}{2a}$	2θ (degrees)
111	0.327	38.151
200	0.377	44.342
220	0.534	64.510
311	0.626	77.482
222	0.654	81.632
400	0.755	98.007
331	0.822	110.665
420	0.844	115.095

Table 10: Calculated expectations of 2θ for silver with FCC structure.